Resonator with transverse surface wave on lithium tantalate crystal for applications in viscosity and temperature sensors

Ernest Brzozowski, Beata Stańczyk, Krystyna Przyborowska, Andrzej Kozłowski
Institute of Electronic Materials Technology
133 Wólczynska Str., 01-919 Warsaw, Poland
e-mail: Ernest.Brzozowski@itme.edu.pl

Abstract: The purpose of this work was to calculate and measure transverse surface acoustic wave resonators on 36°YX oriented lithium tantalate crystal as well as to measure of viscosity and temperature of liquids. An attenuation coefficient was used to model the leak of acoustic energy from surface into bulk of the crystal. The latest materials constants were used. Velocity, electromechanical coupling coefficient, reflection coefficient, attenuation coefficient under free and metallized surface, anisotropy coefficient were calculated, the first three of which were measured using synchronous resonator. A good agreement between measurements and calculations were obtained. Double-channel resonator was sensitive to viscosity and density multiplication product of liquid deposited on the metallized area between transducers. The temperature coefficient of frequency (TCF) of the temperature channel was measured.

Key words: synchronous resonator, surface transverse wave, lithium tantalate, $LiTaO_3$, viscosity sensor

Rezonator z poprzeczną falą powierzchniową na krysztale tantalanu litu do zastosowań w czujnikach lepkości i temperatury cieczy

Streszczenie: Celem pracy były obliczenia i pomiary parametrów poprzecznej akustycznej fali powierzchniowej w rezonatorze na krysztale tantalanu litu o orientacji 36°YX oraz pomiary lepkości i temperatury cieczy. Odpromieniowanie energii akustycznej od powierzchni do objętości kryształu zamodelowano wprowadzając współczynnik tłumienia fali różny od zera. Przyjęto najnowsze dostępne w literaturze stałe materiałowe tantalanu litu. Obliczono prędkość i współczynnik sprzężenia elektromechanicznego, współczynnik odbicia od pojedynczej elektrody, współczynnik tłumienia przy powierzchni swobodnej i metalizowanej oraz współczynnik anizotropii. Z wykorzystaniem rezonatora synchronicznego wykonano pomiary trzech pierwszych wielkości. Uzyskano dobrą zgodność pomiarów z obliczeniami. Skonstruowano dwukanałowy rezonator czuły na iloczyn lepkości i gęstości cieczy osadzonej na metalizowanej powierzchni międzyprzetwornikowej. Zbadano temperaturowy współczynnik częstotliwości (TWCz) kanału przeznaczonego do pomiaru temperatury.

Słowa kluczowe: rezonator synchroniczny, poprzeczna fala powierzchniowa, tantalan litu, $LiTaO_3$, czujnik lepkości

1. Introduction

Acoustic waves are differed by vibration character, planes of mechanical displacements symmetry of medium particles and they may appear in various modes. Mechanical displacements of the wave are described by four parameters. These are the three components of mechanical displacements vector: longitudinal u_1, transverse horizontal u_2, transverse vertical u_3 and the electric potential φ (Fig. 1a). The displacements amplitudes depends on the type of wave and the medium in which the wave propagates. In this work we investigated properties of surface acoustic wave with dominating transverse displacement components u_2 (transverse SAW) in lithium tantalate crystal with orientation 36°YX (Fig. 1b) are investigated.

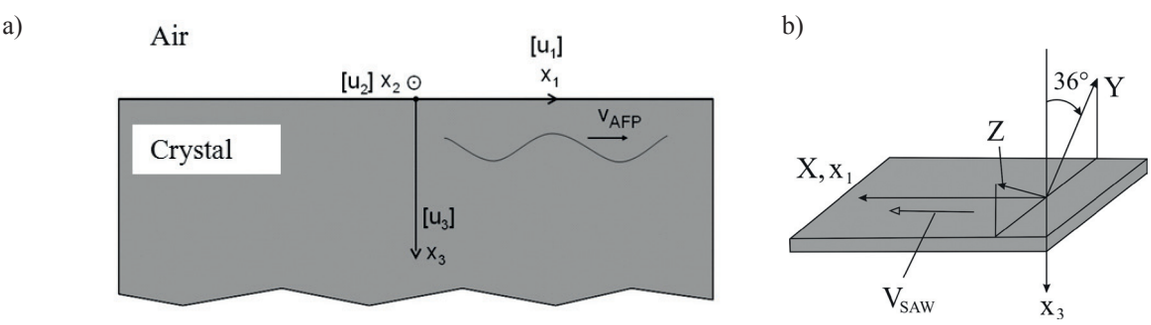

Fig. 1. Components [u_1, u_2, u_3] of particles displacements (a), orientation 36°YX (b), (x_1, x_2, x_3) – coordination system related to wave, (X, Y, Z) – coordination system related to crystal.
Rys. 1. Składowe [u_1, u_2, u_3] przemieszczeń cząstek ośrodka (a), orientacja 36°YX (b), (x_1, x_2, x_3) – układ odniesienia związany z falą, (X, Y, Z) – układ odniesienia związany z kryształem.

http://rcin.org.pl

2. Calculations of SAW parameters

2.1. Calculation method

Arbitrary wave that propagate in piezoelectric medium fulfils the following equations:

$$c_{ijkl}\frac{\partial^2 u_k}{\partial x_l \partial x_i} + e_{kij}\frac{\partial^2 \varphi}{\partial x_k \partial x_i} = \frac{\partial^2 u_j}{\partial t^2}, \tag{1}$$

$$e_{ikl}\frac{\partial^2 u_k}{\partial x_l \partial x_i} - \varepsilon_{ik}\frac{\partial^2 \varphi}{\partial x_k \partial x_i} = 0, \tag{2}$$

where c_{ijkl} - mechanical stiffness tensor, e_{kij} - piezoelectric tensor, ε_{ik} is electric permittivity tensor, t is time.

In algorithm [1] the harmonic solutions of (1) - (2) equations are assumed with no attenuation. To calculate transverse SAW parameters, it is necessary to introduce non-zero imaginary attenuation coefficient γ which describes the wave attenuation along propagation direction x_1:

$$u_j = \beta_j \cdot \exp\left(-\alpha\frac{\omega x_3}{v}\right)\cdot \exp(\mathrm{i}\omega t)\cdot \exp\left[-\mathrm{i}\omega(1-\mathrm{i}\gamma)\frac{x_1}{v}\right], \quad j = 1,2,3 \tag{3}$$

$$\varphi = \beta_4 \cdot \exp\left(-\alpha\frac{\omega x_3}{v}\right)\cdot \exp(\mathrm{i}\omega t)\cdot \exp\left[-\mathrm{i}\omega(1-\mathrm{i}\gamma)\frac{x_1}{v}\right], \tag{4}$$

where β_j, β_4 - displacement amplitudes of medium particles and electric potential, α - the wave attenuation along x_3 direction (into the medium), ω - angular frequency, v - the SAW velocity. After putting (3) - (4) to (1) - (2) a homogeneous system of equations is achieved:

$$\mathrm{MAT}*\beta^T = 0 \tag{5}$$

where: T - transposition, MAT - symmetrical matrix given by:

$$\mathrm{MAT} = \mathrm{MAT\_2} + \mathrm{MAT\_1} + \mathrm{MAT\_0} \tag{6}$$

where:

$$\mathbf{MAT\_2} = \begin{bmatrix} c_{55} & c_{45} & c_{35} & e_{35} \\ & c_{44} & c_{34} & e_{34} \\ & & c_{33} & e_{33} \\ & & & -\varepsilon_{33} \end{bmatrix}\cdot \alpha^2 \tag{7}$$

$$\mathbf{MAT\_1} = \begin{bmatrix} 2c_{15} & (c_{14}+c_{56}) & (c_{13}+c_{55}) & (e_{15}+e_{31}) \\ & 2c_{46} & (c_{36}+c_{45}) & (e_{14}+e_{36}) \\ & & 2c_{35} & (e_{13}+e_{35}) \\ & & & -2\varepsilon_{13} \end{bmatrix}\cdot \mathrm{i}\alpha\cdot \mathrm{i}\gamma \tag{8}$$

$$\mathbf{MAT\_0} = \begin{bmatrix} (-c_{11}+\rho v^2) & -c_{16} & -c_{15} & -e_{11} \\ & (-c_{66}+\rho v^2) & -c_{56} & -e_{16} \\ & & (-c_{55}+\rho v^2) & e_{33} \\ & & & \varepsilon_{11} \end{bmatrix}\cdot (\mathrm{i}\gamma)^2 \tag{9}$$

where c_{IJ} $I, J = 1,2,...,6$ and e_{iJ} $i = 1,2,3$ are material tensors with abbreviated subscripts that are rotated in accordance with crystal orientation, ρ is crystal density. The evolving of (5) determinant yields 8th order polynomial with complex coefficients B_m, ($m = 0,...,8$), which are a function of velocity v, coefficient γ and material tensors:

$$B_8\alpha^8 + B_7\alpha^7 + B_6\alpha^6 + B_5\alpha^5 + B_4\alpha^4 + B_3\alpha^3 + B_2\alpha^2 + B_1\alpha^1 + B_0 = 0 \tag{10}$$

Three roots with positive real parts are chosen from eight complex roots of polynomial (10). The roots must satisfy the condition of decaying amplitude along x_3 direction:

$$Re(\alpha^{(k)}) > 0 \quad k = 1, ..., 3 \tag{11}$$

One root must have negative real part:

$$Re(\alpha^{(4)}) < 0 \tag{12}$$

for mathematical modeling of partial leakage of acoustic energy inside the crystal.

The equation system (5) is solved for every $\alpha^{(k)}$, $k = 1, ..., 4$ root obtaining set of parameters $\beta_j^{(k)}$ ($j, k = 1,...,4$). One parameter β is set arbitrary non-zero value in each of the four solutions. A three order minor is chosen from matrix in equation (5). Putting $\alpha^{(k)}$ and β_j(k) ($j, k = 1,..., 4$) to wave equations (3) - (4) yields:

$$u_j = \sum_{k=1}^{4} A^{(k)}\beta_j^{(k)}\cdot \exp\left(-\alpha^{(k)}\frac{\omega x_3}{v}\right)\cdot \exp(\mathrm{i}\omega t)\cdot \cdot \exp\left[-\mathrm{i}\omega(1-\mathrm{i}\gamma)\frac{x_1}{v}\right], \tag{13}$$

$$\varphi = \sum_{k=1}^{4} A^{(k)}\beta_j^{(k)}\cdot \exp\left(-\alpha^{(k)}\frac{\omega x_3}{v}\right)\cdot \exp(\mathrm{i}\omega t)\cdot \cdot \exp\left[-\mathrm{i}\omega(1-\mathrm{i}\gamma)\frac{x_1}{v}\right], \tag{14}$$

where $A^{(k)}$ are parameters. Putting (13) - (14) to free surface boundary conditions yields homogeneous system of equations with variable $A^{(k)}$:

$$\sum_{k=1}^{4}\left[\beta_1^{(k)}\left[i\gamma c_{15}+\alpha^{(k)}c_{55}\right]+\beta_2^{(k)}\left[i\gamma c_{56}+\alpha^{(k)}c_{45}\right]+ +\beta_3^{(k)}\left[i\gamma c_{55}+\alpha^{(k)}c_{35}\right]+\beta_4^{(k)}\left[i\gamma e_{15}+\alpha^{(k)}e_{35}\right]\right]\cdot A^{(k)} = 0 \tag{15}$$

http://rcin.org.pl

$$\sum_{k=1}^{4}\left[\beta_1^{(k)}\left[i\gamma c_{14}+\alpha^{(k)}c_{45}\right]+\beta_2^{(k)}\left[i\gamma c_{46}+\alpha^{(k)}c_{44}\right]+\right.$$
$$\left.+\beta_3^{(k)}\left[i\gamma c_{45}+\alpha^{(k)}c_{34}\right]+\beta_4^{(k)}\left[i\gamma e_{14}+\alpha^{(k)}e_{34}\right]\right]\cdot A^{(k)}=0 \quad (16)$$

$$\sum_{k=1}^{4}\left[\beta_1^{(k)}\left[i\gamma c_{13}+\alpha^{(k)}c_{35}\right]+\beta_2^{(k)}\left[i\gamma c_{36}+\alpha^{(k)}c_{34}\right]+\right.$$
$$\left.+\beta_3^{(k)}\left[i\gamma c_{35}+\alpha^{(k)}c_{33}\right]+\beta_4^{(k)}\left[i\gamma e_{13}+\alpha^{(k)}e_{33}\right]\right]\cdot A^{(k)}=0 \quad (17)$$

$$\sum_{k=1}^{4}\left[\beta_1^{(k)}\left[i\gamma e_{31}+\alpha^{(k)}e_{35}\right]+\beta_2^{(k)}\left[i\gamma e_{36}+\alpha^{(k)}e_{34}\right]+\right.$$
$$\left.+\beta_3^{(k)}\left[i\gamma e_{35}+\alpha^{(k)}e_{33}\right]-\beta_4^{(k)}\left[i\gamma\varepsilon_{13}+\alpha^{(k)}\varepsilon_{33}+\varepsilon_0\right]\right]\cdot A^{(k)}=0 \quad (18a)$$

For electrically shorted surface (metallized) instead of (18a) stands:

$$\sum_{k=1}^{4}\beta_4^{(k)}\cdot A^{(k)}=0. \quad (18b)$$

The determinant W of (15) - (18) equations system depends on material tensors and two variables: the velocity v and coefficient γ. The velocity v and coefficient γ are determined from two dimensional minimum of determinant W. The velocity v is a phase velocity.

The electromechanical coupling coefficient is given by the following dependence:

$$K^2=\frac{2\,(v_f-v_m)}{v_f}, \quad (19)$$

where v_f and v_m are velocity under free and metallized surface, respectively.

The reflection coefficient of single electrode was calculated from dependence [2]:

$$r=0.55\cdot K^2, \quad (20)$$

which is true under conditions of infinitesimally thin metallization and strong electromechanical coupling in lithium tantalate. The wave attenuation coefficient in dimensions dB/λ (where λ is a wavelength) is related to coefficient γ by the following:

$$\delta=54.575\cdot\gamma. \quad (21)$$

Acoustic power flow angle was calculated from a difference between phase and group velocity [2]:

$$\phi=\theta-\psi, \quad (22)$$

where θ is angle between X axis and phase velocity direction, while ψ was determined from slowness curve $1/v = f(\theta)$ under change of θ about $d\theta$, where $d\theta = 0.1°$. There is a computer program implementing (1) - (22) formulas.

Theoretical AFP velocity and attenuation coefficient changes induced by interaction with Newtonian liquid are given by the dependencies derived from small perturbation analysis [7]:

$$\Delta\delta=k\cdot\frac{v v_2^2\sqrt{\pi\cdot f}}{8\pi\cdot f\cdot P}\left(\sqrt{\eta'\cdot\rho'}+\sqrt{\eta\cdot\rho}\right), \quad (23)$$

$$\Delta v=-\frac{v^2 v_2^2\sqrt{\pi\cdot f}}{8\pi\cdot f\cdot P}\left(\sqrt{\eta'\cdot\rho'}-\sqrt{\eta\cdot\rho}\right), \quad (24)$$

where: η and η', ρ and ρ' - liquid viscosity and density before and after surface perturbation, respectively, v_2 - horizontal component displacement velocity, f - frequency, P - power flow angle module, k - wave vector module.

2.2. Calculation results

Parameters of SAW velocity under free and metallized surface, electromechanical coupling coefficient, attenuation coefficients under free and metallized surface, acoustic power flow angle and anisotropy coefficient $\partial\phi/\partial\theta$ were calculated from (1) - (22). Partial displacement amplitudes distributions along x_3 axis were calculated for free and metallized crystal surface. The calculations were made using four sets of material constants available in literature [3 - 6]. The results obtained for particular material constants sets are shown in Tab. 1.

Velocity under free and metallized surface oscillated from 4171 to 4226 m/s and from 4077 to 4112 m/s, respectively. Electromechanical coupling and reflection coefficients were from 4.54 to 5.56% and from 2.50 to 3.06%, respectively. Attenuation coefficients under free and metallized surface varied from 2.5 to 21 and from 11 to 79×10^{-5} dB/λ, respectively. Attenuation coefficient turned out to be higher for free surface than for metallized surface only for materials constants [6]. Forward calculations and measurements are in good agreement with this result. Acoustic power flow angle was zero for all of the materials sets, while diffraction anisotropy coefficient $\partial\phi/\partial\theta$ varied from 2.44 to 2.74.

Amplitude displacement distributions under free and metallized surface are shown in Figs. 2a and b. Component u_2 – transverse horizontal is dominating. The electric conditions on the crystal surface determine the wave penetration distance. Under free surface the penetration distance becomes 15 times higher than under the metallized surface. The high penetration distance means that there is acoustic power leakage from surface into the crystal bulk. The surface metallization (electric short) induces energy concentration in the surface vicinity.

SAW velocity and attenuation coefficient changes versus liquid viscosity density product are shown in Fig. 3.

http://rcin.org.pl

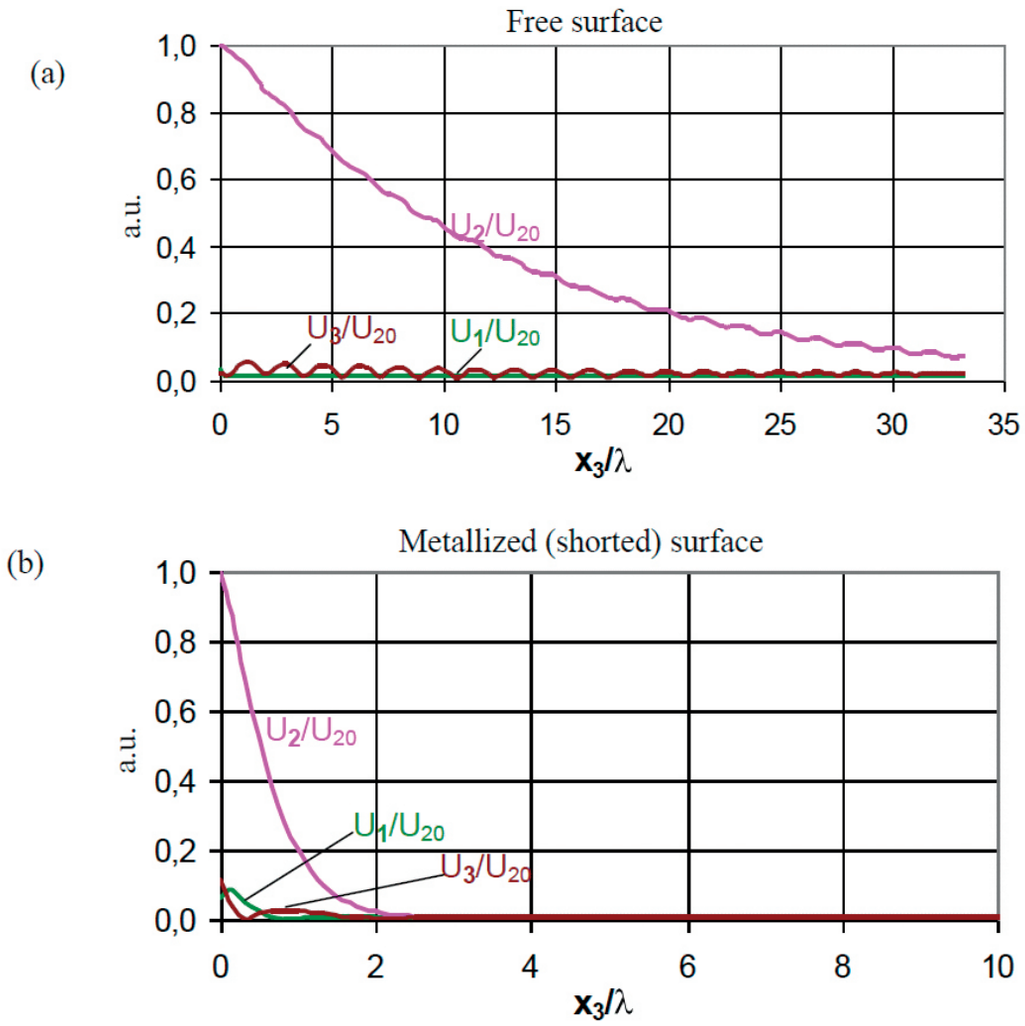

Fig. 2. Displacement amplitudes under free: – (a) and metallized (shorted) – (b) surface.
Rys. 2. Amplitudy przemieszczeń cząstkowych przy powierzchni swobodnej – (a) i zwartej elektrycznie (metalizowanej) – (b).

Tab. 1. Transverse SAW parameters calculations results.
Tab. 1. Wyniki obliczeń parametrów poprzecznej AFP.

36°YX $LiTaO_3$	**[3]**	**[4]**	**[5]**	**[6]**
v_f [m/s]	4 171.7	4 211.3	4 226.3	4 214.5
v_m [m/s]	4 077.1	4 112.8	4 108.8	4 105.4
δ_f [dB/l]×10^{-5}	3,9	2,5	21	17
δ_m [dB/l]×10^{-5}	16	79	26	11
K^2 [%]	4.54	4.67	5,56	5.18
r [%]	2.50	2.57	3.06	2.85
f [°]	0.0	0.0	0.0	0.0
$\partial f/\partial\theta$	2.44	2.61	2.74	2.68

http://rcin.org.pl

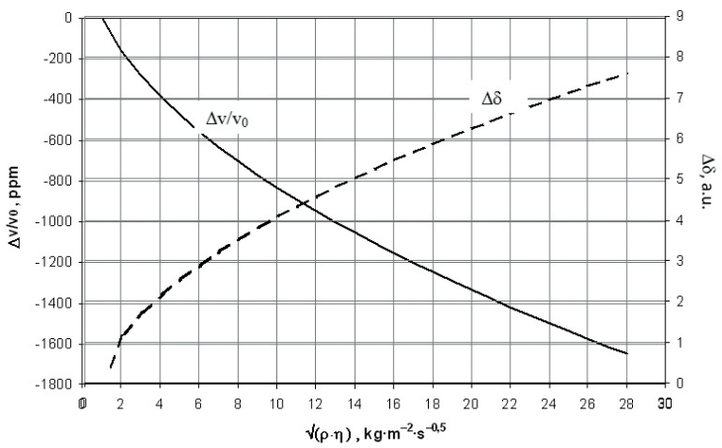

Fig. 3. Theoretical changes of transverse SAW velocity ($\Delta v/v_0$) and attenuation coefficient ($\Delta\delta$) as a function of the root of viscosity and density product.
Rys. 3. Teoretyczne zmiany prędkości ($\Delta v/v_0$) i współczynnika tłumienia fali poprzecznej AFP ($\Delta\delta$) w funkcji pierwiastka iloczynu lepkości i gęstości cieczy.

3. Measurements

3.1. Measurements of SAW parameters

A multimode synchronous rezonator was applied for transverse SAW measurements. The resonator (Fig. 4) data are: W = 1.5 mm, d = 2.99 mm, p = 27.6 μm, N_t = 5 i N_r = 200, where W stands for aperture, d - distance between transducers, p - electrode period, N_t - electrode number of interdigital transducer and N_r - electrode number of reflector.

The resonator metallization was deposited on 36°YX lithium tantalite, the aluminium thickness h_{Al} was about 0.1 μm. The measured amplitude response of the resonator is shown in Fig. 5. Shorted measurement circuit showed insertion loss about 1.2 dB. The amplitude response was measured using Agilent network analyzer 8753ET.

Two resonances are related to two vibration modes in the resonator. SAW parameters were determined from the comparison of the measured amplitude response with the calculated one. The velocity in periodically metallized interdigital area amounted to about 4136 ± 2 m/s, the velocity in continuously metallized area about 4101 ± 2 m/s, the electromechanical coupling coefficient about 2.35 ± 0.1%. Determination of SAW velocity under free surface requires evaluation of the influence of metallization thickness. A resonator with metallization thickness h_{Al} about 0.2 μm was fabricated for this purpose. Determined SAW velocity under continuous metallization came to about 4106 ± 3 m/s and under periodical metallization to about 4140 ± 3 m/s. Below $h_{Al}/\lambda = 3{,}6 \cdot 10^{-3}$ ratio the velocity changes are linear with metallization thickness. Using (19) the determined velocity under free surface was noted to be about 4215 ± 15 m/s. High inaccuracy of the determination is due to the combination of SAW velocities and electromechanical coupling coefficient measurement inaccuracies. The measured SAW parameters are compared to the calculated ones in Tab. 2. The best measurement and calculation compatibility was obtained for material constants [6].

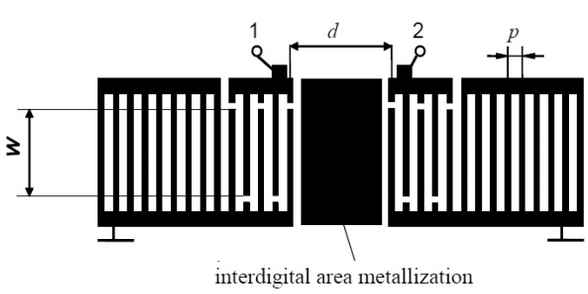

Fig. 4. Synchronous rezonator structure.
Rys. 4. Struktura rezonatora synchronicznego.

Tab. 2. Comparison between measured and calculated SAW parameters in 36°YX $LiTaO_3$.
Tab. 2. Porównanie obliczonych i zmierzonych parametrów AFP w 36°YX $LiTaO_3$.

36°YX $LiTaO_3$	[5] 1990	[6] 1999	Measured in ITME 2013
v_f [m/s]	4 226.3	4 214.5	4215 ± 15
v_m [m/s]	4 108.8	4 105.4	4106 ± 3
K^2 [%]	5.56	5.18	5.2 ± 0.1
r [%]	3.06	2.85	2.35 ± 0.1

http://rcin.org.pl

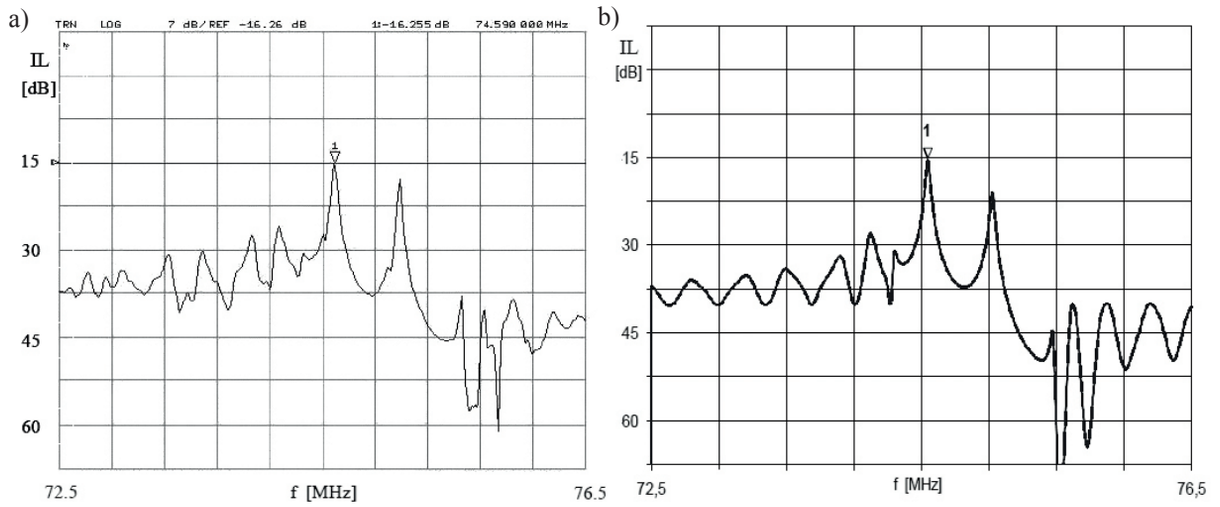

Fig. 5. Amplitude response of the resonator as a function of frequency: a) measured, b) calculated.
Rys. 5. Charakterystyki amplitudowe rezonatora w funkcji częstotliwości: a) zmierzone, b) obliczone.

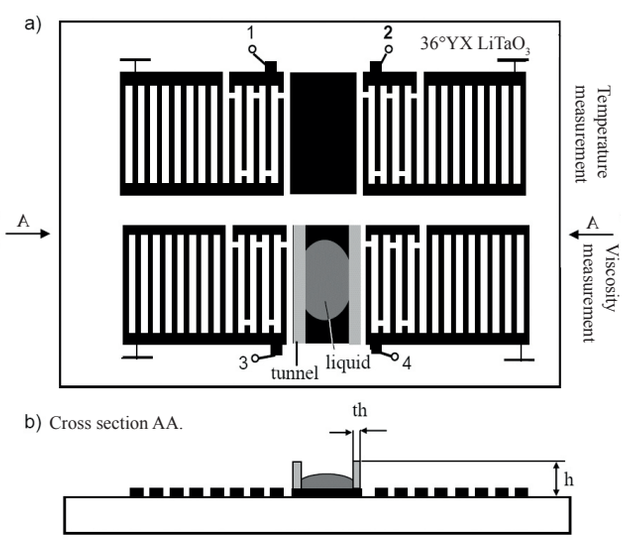

Fig. 6. Double channel rezonator, top view (a), cross section (b).
Rys. 6. Rezonator dwukanałowy, widok z góry (a), przekrój (b).

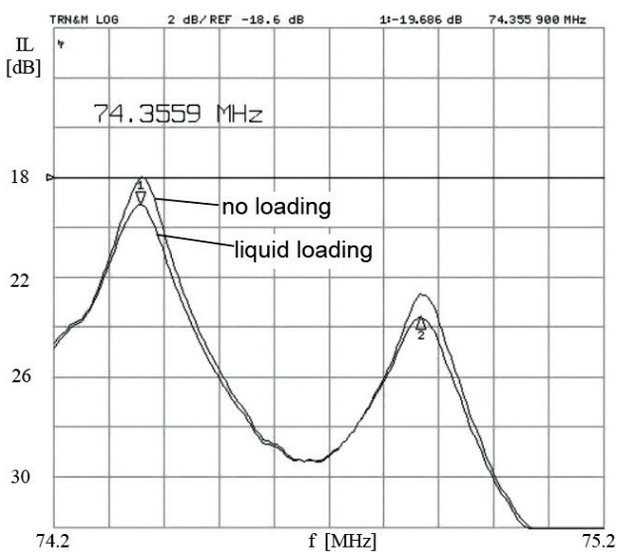

Fig. 7. The influence of liquid loading on to amplitude response in the frequency range of 74.2 - 75.2 MHz.
Rys. 7. Wpływ dociążenia cieczą na charakterystykę amplitudową rezonatora w zakresie częstotliwości 74,2 - 75,2 MHz.

3.2. Measurements of viscosity and temperature

A water-glycerine solution was used to investigate transverse SAW interaction with liquid loading. In this case the viscosity is a known function of solution concentration and temperature. The measurements were carried out with the double channel resonator. The interdigital areas designed for the liquid loading were metallized in both channels (Fig. 6). The tunnel made of quartz was applied for shielding the transducer against liquid loading. Mounted with epoxy, the glue tunnel was about 2 mm high and about 0.5 mm thick.

Water glycerine solution was deposited using micropipette. After loading the interdigital area the insertion loss rose, while the resonance frequency was decreased (Fig. 7).

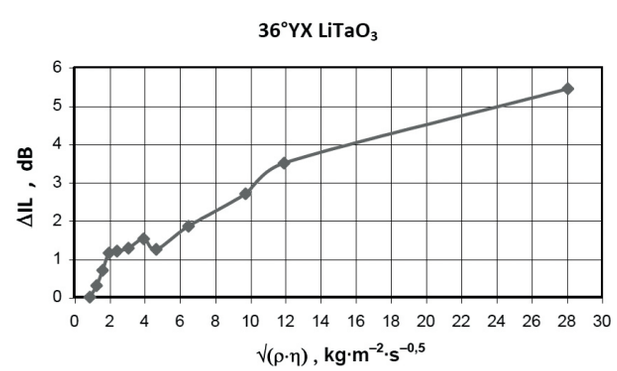

Fig. 8. Insertion loss changes of resonator versus root of viscosity and density product.
Rys. 8. Zmiany tłumienności wtrąceniowej rezonatora w funkcji pierwiastka z iloczynu lepkości i gęstości.

http://rcin.org.pl

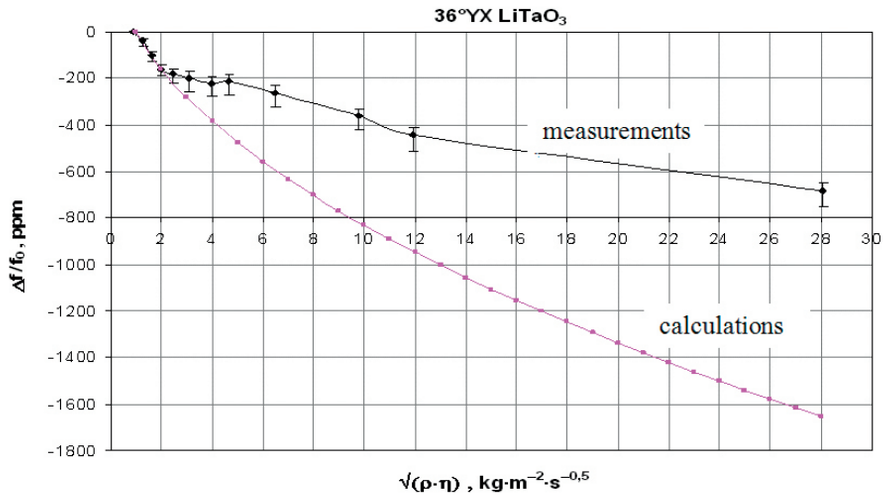

Fig. 9. Changes of resonance frequency as a function of the root of viscosity and density product.
Rys. 9. Zmiany częstotliwości rezonansowej w funkcji pierwiastka iloczynu lepkości i gęstości cieczy.

Tab. 3. The results of measurements of rezonator's parameters versus loading solution concentration.
Tab. 3. Pomiary parametrów rezonatora w funkcji stężenia roztworu obciążającego.

Loading 30°C	ρ [g/cm³]	η [mPa·s]	$\sqrt{(\rho\cdot\eta)}$	Concentration [%]	A_1 [dB]	f_1 [MHz]	ΔA_1 [dB]	Δf_1 [kHz]
water	1.00000	0.8	0.894427	0	-19.7	74.3559	0.0	0.00000
Water-glycerine solution	1.0586	1.541	1.277225	24	-20	74.353	0.3	-39.00161
	1.09245	2.427	1.628305	37	-20.4	74.3485	0.7	-99.52136
	1.1165	3.54	1.988067	46	-20.85	74.344	1.2	-160.04110
	1.13815	5.21	2.43511	54	-20.9	74.3425	1.2	-180.21435
	1.1601	8.26	3.095549	62	-20.98	74.341	1.3	-200.38760
	1.17935	13.27	3.956005	69	-21.22	74.3395	1.5	-220.56084
	1.1821	14.32	4.114325	70	-21.26	74.338	1.6	-240.73409
	1.19025	18.34	4.672171	73	-20.95	74.34	1.3	-213.83643
	1.19565	21.68	5.091335	75	-21.39	74.335	1.7	-281.08059
	1.20925	34.92	6.498231	80	-21.78	74.332	2.1	-321.42708
	1.20925	34.92	6.498231	80	-21.55	74.3365	1.9	-260.90734
	1.2279	77.5	9.755114	87	-22.4	74.329	2.7	-361.77358
	1.23585	115.3	11.93706	90	-23.2	74.323	3.5	-442.46657
Glycerine	1.26201	624	28.06233	100	-25.14	74.305	5.4	-684.54554

http://rcin.org.pl

The results of the mesurements of rezonator's parameters against solution concentration are given in Tab. 3. In Fig. 8 - 9 the changes of resonators parameters are showed as a function of root of viscosity and density product.

Temperature coefficient of frequency (TCF) was determined from measurements of resonance frequency changes in the temperature channel. For temperature stabilization a precision thermostat ITR-200 was applied and a constant phase method was used [9]. Relative frequency changes Df/f measured in 20.. 80°C range were linear with TCF = – 26 (±1) ppm/°C.

4. Conclusions

Transverse horizontal displacements dominate in SAW in 36°YX $LiTaO_3$. SAW power leaks into the crystal bulk under free surface. Power concentration in the surface vicinity could be achieved by electrical short of the surface.The resonator operates properly when the interdigital area is metallized. Materials constants from [6] give calculations results in agreement with measurements results. Liquid loading of the interdigital area introduces systematic changes of the insertion loss and resonance frequency. Parameter changes are nonlinear and are not predicted by a small perturbation theory in most ranges of the investigated viscosities. The changes could be predicted only in the range from 0 to 2 $kg \cdot m^{-2} \cdot s^{-0.5}$ and in this range the rezonator can be a promising application for viscosity and temperature measurements.

5. References

[1] Nakamura K., Kazumi M., Shimizu H.: SH-type and Rayleigh-type surface waves on rotated Y-cut $LiTaO_3$, *IEEE Ultrason. Symp,* 1977, 819 − 822

[2] Meyer H., Russer P.: Analysis of leaky surface waves on $LiTaO_3$ substrate, *IEEE Frequency Control Symposium*, 1992, 378 – 383

[3] Warner A. W., Onoe M., Coquin G. A.: Determination of elastic and piezoelectric constants for crystals in class (3m), *J. Acoust. Soc*. Amer., 1967, 42, 1223 – 1231

[4] Smith R. T., Welsh F. S.: Temperature dependence of the elastic, piezoelectric, and dielectric constants of lithium tantalate and lithium niobate, *J. Appl. Phys*., 1971, 42, 2219 – 2230

[5] Kovacs G., Anhorn M., Engan H. E.: Improved material constants for $LiNbO_3$ and $LiTaO_3$, *Proc. 1990 IEEE Ultrason. Symp*., 1990., 435 – 438

[6] Kushibiki J., Takanaga I., Arakawa M.: Accurate measurements of the acoustical physical constants of $LiNbO_3$ and $LiTaO_3$ single crystals, *IEEE Trans. Ultrason. Ferroelectr. Freq. Control*, 1999, 46, 5, 1315 – 1323

[7] Shiokawa S., Kondoh J.: Surface acoustic wave sensor for liquid-phase application, *IEEE Ultrasonics Symposium*, 1999, 445 – 452

[8] Soluch W.: Application of synchronous two-port resonators for measurement of SAW parameters in piezoelectric crystals, *IEEE Trans. Ultrason. Ferroelect. Freq. Contr.,* 1998 ,45 , 4, 1113

[9] Brzozowski E., Soluch W.: SAW and pseudo SAW properties of $NdCa_4O(BO_3)_3$ crystal, *Electr. Lett.*, 2008, 44, 1, 64 – 65

http://rcin.org.pl